A Characterization of Tropical Transient Activity in the CAM3 Atmospheric Hydrologic Cycle

PHILIP J. RASCH,* MARK J. STEVENS,* LUCREZIA RICCIARDULLI,+ AIGUO DAI,* ANDREW NEGRI,#
ROBERT WOOD,@ BYRON A. BOVILLE,* BRIAN EATON,* AND JAMES J. HACK*

*National Center for Atmospheric Research,& Boulder, Colorado
+ Remote Sensing Systems, Santa Rosa, California
# Laboratory for Atmospheres, NASA GSFC, Greenbelt, Maryland
@ Department of Atmospheric Sciences, University of Washington, Seattle, Washington

(Manuscript received 24 January 2005, in final form 7 September 2005)

ABSTRACT

The Community Atmosphere Model version 3 (CAM3) is the latest generation of a long lineage of general circulation models produced by a collaboration between the National Center for Atmospheric Research (NCAR) and the scientific research community. Many aspects of the hydrological cycle have been changed relative to earlier versions of the model. It is the goal of this paper to document some aspects of the tropical variability of clouds and the hydrologic cycle in CAM3 on time scales shorter than 30 days and to discuss the differences compared to the observed atmosphere and earlier model versions, with a focus on cloud-top brightness temperature, precipitation, and cloud liquid water path. The transient behavior of the model in response to changes in resolution to various numerical methods used to solve the equations for atmospheric dynamics and transport and to the underlying lower boundary condition of sea surface temperature and surface fluxes has been explored.

The ratio of stratiform to convective rainfall is much too low in CAM3, compared to observational estimates. It is much higher in CAM3 (10%) than the Community Climate Model version 3 (CCM3; order 1%–2%) but is still a factor of 4–5 too low compared to observational estimates. Some aspects of the model transients are sensitive to resolution. Higher-resolution versions of CAM3 show too much variability (both in amplitude and spatial extent) in brightness temperature on time scales of 2–10 days compared to observational estimates. Precipitation variance is underestimated on time scales from a few hours to 10 days, compared to observations over ocean, although again the biases are reduced compared to previous generations of the model. The diurnal cycle over tropical landmasses is somewhat too large, and there is not enough precipitation during evening hours. The model tends to produce maxima in precipitation and liquid water path that are a few hours earlier than that seen in the observations over both oceans and land.

1. Introduction

Transient activity in cloud processes and precipitation is an important component of the atmosphere and the Earth's climate. Indeed, clouds are by their very nature transient. Yet, it is a frequent experience with general circulation models (GCMs) that clouds' transient aspects are quite different from those seen in the atmosphere (Ricciardulli and Garcia 2000; Dai and Trenberth 2004; Scinocca and McFarlane 2004; Yang and Slingo 2001), even when the spatial patterns are reasonable.

When viewed from the larger scale (>100 km), there is both a stochastic component to clouds, as well as a component that is strongly correlated with other meteorologically important features. Clouds show variations on time scales varying from seconds to decadal lengths. This paper focuses on aspects of clouds associated with time scales shorter than a month. Longer time-scale features are discussed in Boville et al. (2006) and Hack et al. (2006b).

The shorter time-scale properties of clouds are important to the climate system for a variety of reasons. On the shortest of the time scales resolvable by large-

& The National Center for Atmospheric Research is sponsored by the National Science Foundation.

Corresponding author address: Dr. Philip J. Rasch, National Center for Atmospheric Research, P.O. Box 3000, Boulder, CO 80307-3000.
E-mail: pjr@ucar.edu

scale models (order an hour to a day), clouds are involved in rapid transports of heat, moisture, momentum, and atmospheric trace constituents. In the Tropics, where nearly all of the solar variance is diurnal (as opposed to seasonal), clouds act as the strongest modulators of the variability associated with solar forcing (Bergman and Salby 1996). The vigorous motions associated with latent heat release can introduce oscillations in the atmosphere that propagate to and influence regions far from their source (Ricciardulli and Garcia 2000). The breaking of gravity waves excited by convection can drive major modes of the middle atmosphere like the semiannual and quasi-biennial oscillation (QBO; e.g., Takahashi 1999). On longer time scales cloud features participate strongly in regulating and interacting with other dynamical features like squall lines, Madden–Julian oscillations (MJOs), midlatitude frontal storms, and a host of other atmospheric phenomena.

In regions of the atmosphere where latent heat release drives atmospheric dynamics less strongly, clouds play other roles. Their modulation of solar insolation and the radiative cooling near cloud top act to strongly influence the atmospheric boundary layer. The transports of heat and moisture throughout the boundary layer are thus strongly modulated by clouds, and this in turn plays a role in the venting of other important trace constituents, like water, through short-lived species, (CH3I, radon, to long-lived species like CO_2). The role of the boundary layer and convective processes in rectification of trace species (e.g., Denning et al. 1996) and transport are discussed in more detail in Rasch et al. (2006) elsewhere in this issue.

Many of the diagnostics similar to those employed in this paper have been used before to analyze earlier versions of the National Center for Atmospheric Research (NCAR) GCMs and climate models. Ricciardulli and Garcia (2000) described the response of equatorial waves to deep convective forcing in the Community Climate Model version 3 (CCM3). Collier and Bowman (2004) described the behavior of the diurnal variation of tropical precipitation in CCM3, using prescribed ocean surface temperatures. Ricciardulli and Sardeshmukh (2002) documented the local time and space scales of organized convection using satellite retrievals of a proxy for convection and compared those results to CCM3 and another model. Dai and Trenberth (2004) documented the behavior of the diurnal variation of precipitation, clouds, and other fields in the Community Climate System Model version 2 (CCSM2), a coupled model which utilized the Community Atmosphere Model version 2 (CAM2) for its atmospheric component. The atmospheric GCM communicated with the ocean model component of the coupled system once per day. This restricted the ability of the ocean surface to respond to changes in the forcing, and thus affected the diurnal variation of convection and precipitation. Dai and Trenberth (2004) attributed part of the weak diurnal variation in the CAM2 over oceans to this lack of a diurnal variation in surface temperature and fluxes.

Although many of the papers cited in the previous paragraph are quite recent, CCM3 was released in 1996 and CAM2 was released in 2001, and a variety of important changes have occurred in our model framework in the years since. These changes have the potential to alter the variability of the cloud processes in the model, and the response of the model to changes in variability. In addition to changes in model physics and dynamics, the model can be run in a much broader variety of configurations than previous versions of our GCM. This allows us to examine the sensitivity of the transient aspects of clouds to resolution, lower boundary conditions, and formulation for large-scale dynamics. It is the goal of this paper to document some aspects of the simulation of cloud variability in the Community Atmosphere Model version 3 (CAM3) to these variations, and to contrast CAM3's behavior with the behavior of previous generations of the model.

2. Description of CAM3 configurations

Since a description of components of CAM3 can be found in other papers appearing in this special issue, we point the reader to the relevant papers describing the components, and highlight changes to our GCM from the CCM3 version that can influence the model variability.

A general overview of the CAM3 is provided in Collins et al. (2006). The formulation for the hydrologic cycle can be found in Boville et al. (2006). The climatological (seasonal and longer) time-scale features of the hydrologic cycle simulation can be found in Hack et al. (2006b). The sensitivity of the model to horizontal resolution is discussed in Hack et al. (2006a). The use of the slab ocean, which allows the sea surface to respond to changes in fluxes at the ocean surface, is discussed in Kiehl et al. (2006). Full details of all aspects of the formulation can be found in Collins et al. (2004).

It is worthwhile to discuss some changes that could influence the model cloud variability and to highlight some areas that remain unchanged that also may affect it. CCM3 used a prescribed cloud water formulation. The cloud condensate distribution was specified to be a simple function of the vertical integral of water vapor.

TABLE 1. The cases examined in this study, ordered from lowest to highest resolution. Note that although the semi-Lagrangian and spectral T42 models contain the same number of grid points, the former model does not use the inherent smoothing required for a spectral transform model. FD stands for finite difference.

Case	Resolution	Dynamics	SST	Time step (s)
T42amip	128 × 64	Spectral/FD	Prescribed 1950–54	1200
T42som	128 × 64	Spectral/FD	Predicted SST	1200
SLDamip	128 × 64	Semi-Lagrangian/FD	Prescribed 1950–54	3600
FVsom	144 × 91	Control volume	Predicted SST	1800
FVamip	144 × 91	Control volume	Prescribed 1950–54	1800
T85amip	256 × 128	Spectral/FD	Prescribed 1950–54	600

The latent heat of fusion associated with phase change between ice and liquid was ignored. CAM2 and CAM3 employ a prognostic cloud condensate parameterization. The CAM2 employed a simpler condensate variable that distinguished less strongly between water and ice and rain and snow. CAM2 also neglected latent heat of fusion, advection and sedimentation of condensate, and some evaporation terms. CAM3 condensed water substances represented in the model include the following:

- small liquid and ice particles that evolve dynamically in response to advection, conversion to precipitating forms, phase changes (between liquid, ice, and vapor), sedimentation, and turbulent transport;
- large liquid and ice particles (rain and snow/graupel) that are assumed to be in steady state with their sources.

In CCM3, convection could only detrain water vapor, and cloud water was insensitive to local detrainment. In CAM3 the convection is allowed to detrain condensate and water vapor, and these fields feed the stratiform clouds. In CCM3 precipitation fell to the surface. In CAM3, precipitation can evaporate as it falls. These features, in addition to changes to radiation, cloud overlap, the land model, and other things, have produced substantial changes to the water vapor, liquid, and ice distributions and the associated radiative and thermodynamic balances, as well as other facets of the model climate between CAM3 and CCM3. Of course, with reformulations of this extent, changes to tunable parameters were also required.

We have examined the transient behavior in six different model configurations described in Table 1. These configurations explore the model sensitivity to resolution, to the method used to calculate the sea surface temperature (SST), and to the numerical method used to solve the atmospheric dynamics. Small changes in a few tunable parameters are required to produce similar climates in the time mean because the solution is sensitive to resolution and numerics when these model aspects are changed. We have not examined the transient sensitivity of the model to changes in these parameters, although the transient behavior of the model may be sensitive to changes to them. Scinocca and McFarlane (2004) have shown that the transient behavior of the Zhang–McFarlane scheme used for deep convection in CAM3 is quite sensitive to the setting of certain constants within that parameterization. Such an exploration is certainly merited, but initially we have decided to document our current formulations. We intend in future studies to explore the sensitivity of our model to parameterization settings, and the parameterizations themselves. Dai and Trenberth (2004) speculated that the global diurnal cycle deficiencies in CCSM2 over ocean were associated in part to the lack of a diurnal cycle in CAM. In most configurations of CAM3 and CCSM the SST is held fixed over each 24-h time period. The standard atmosphere-only versions of CAM3 fix the SST and update it to a value interpolated from monthly mean values read in from an external dataset. In the standard version of the coupled model (CCSM3), CAM3 communicates with the ocean model once per day, and the SSTs are again held fixed for a 24-h period. In the slab ocean model (SOM) configurations, the SSTs are allowed to evolve in time and to respond to changes in the net radiation and surface fluxes associated with changing wind speed. Therefore, the SOM configuration provides an opportunity to explore the sensitivity of the model transient activity to a varying SST. The SOM configuration, however, will underestimate the diurnal variation of SST because it is intended to model the mixed layer, which is much deeper than the top few meters of the ocean that participate strongly in the diurnal variation. Nevertheless this configuration provides some opportunity for the oceans and atmosphere to interact in diurnal time scales. The models labeled with the suffix "AMIP" (Atmospheric Model Intercomparison Project) used prescribed

monthly mean SSTs following Rayner et al. (2003) and Reynolds et al. (2002).

All model versions were started at near equilibrium conditions and run for 5 yr. The versions of the model identified as having a 128 × 64 resolution have horizontal cell dimensions of approximately 2.8 degrees on a side. The Finite Volume (FV) model employs a 2 × 2.5 degree regular latitude–longitude grid with cell centers located at poles and the equator. There are approximately 60% more points on the globe than the 128 × 64 grid model configurations. The T85 model is precisely twice as many points in latitude and longitude as the 128 × 64, for a factor of 4 increase in resolution. Fields were output at 3-h intervals.

3. Convective versus stratiform precipitation

Many interesting cloud features that are associated with convection occur on short time scales, and it is important to identify the partitioning between cloud phenomena undergoing vigorous convection and that associated with the less vigorous motions associated with decaying convective elements and frontal motions. In the Tropics, where more than half the global precipitation occurs, the partitioning is believed to be shared approximately equally between convective and stratiform precipitation (Schumacher and Houze 2003; Houze 1997). The vertical distributions of heating associated with precipitation occur with very different distributions for convective and stratiform processes (Houze et al. 1980). Convective heating is generally believed to be positive throughout the vertical profile, with the height of the maximum depending on the size spectrum of the convective elements, while the heating maximum occurs in the mid- and upper troposphere for stratiform process, with cooling below. Also, the areal extent of the clouds associated with vigorous updrafts is believed to be only a few percent with a much larger radiative contribution from stratiform clouds (LeMone and Zipser 1980; Jorgensen and LeMone 1989). Hartmann et al. (1984) showed that a reasonable large-scale tropical dynamical response to the heat release by tropical precipitation required the correct vertical partitioning of the heating as determined by the partitioning of the convective and stratiform components.

A useful, quantitative global picture of the partitioning between convective and stratiform rainfall estimates can be achieved by comparing observations from the Tropical Measuring Mission (TRMM) Precipitation Radar (PR) to the CAM3 precipitation. Although the PR and TRMM Microwave Imager (TMI) datasets provide some of the best global characterizations of precipitation available today (Kummerow et al. 2000), they are not without deficiencies. TRMM was launched in a precessing orbit that allows relatively complete coverage of the earth between 38°N and 38°S, observing a given location once or twice per day, at a different time each day, with a cycle of about 46 days. Since precipitation is highly variable in space and time, the sampling error is significant. Negri et al. (2002a) have estimated the biases in hourly rain rates for 5 × 5 degree grid estimates to be 15%–48% for PR and 13%–34% for TMI. Negri et al. (2002b) found a bias in TMI of 33% compared to monthly mean regional estimates from rain gauges for the same period. Bowman et al. (2003) found very small biases for TMI and about 30% bias for PR compared to tropical Pacific buoy rain gauge data. Kummerow et al. (2000) showed 24% difference between TMI and PR retrieval of monthly mean estimates of global tropical precipitation. Masunaga et al. (2002) explained these differences in terms of biases in the assumed vertical profiles of cloud water content and ambiguities in the attenuation correction in heavy precipitation around tropical rainfall maxima. These uncertainties result in biases. TMI underestimates the near-surface condensed water in midlatitude winter, and PR underestimates the vertically integrated liquid water amount [liquid water path (LWP)] in the Tropics. The consequence is that PR rain-rate estimates tend to be much lower than TMI rain-rate estimates in the Tropics, while the two are much closer to each other in the extratropics.

Figure 1 shows the annual averaged rainfall estimates for TRMM PR (TRMM dataset 3A25, composited from 1998 to 2003 at about 0.5 degree resolution) and a 5-yr average of the T85 version of CAM. CAM and TRMM total precipitation estimates (lower panels) agree qualitatively. It is easier to compare the simulations quantitatively by examining the zonal precipitation distribution adjacent to the latitude–longitude panels. CAM3 is about 25% higher in the Tropics, and the difference is much smaller in the extratropics. As discussed previously, the TRMM PR retrievals are always lower than the TMI in the Tropics, and the TMI product agrees much more closely with the CAM global total (stratiform plus convective) precipitation (not shown). Although the total precipitation is similar to CAM, the partitioning between stratiform and convective rain is very different. This signal is similar to that seen with CCM3 in Song and Yu (2004). They reported stratiform rain accounting for 1.5% of the total rainfall between 20°N and 20°S. This simulation shows stratiform precipitation to be about 10% of the total rain, which is closer to, but still much lower than, the TRMM estimates. The amount of stratiform rainfall in the

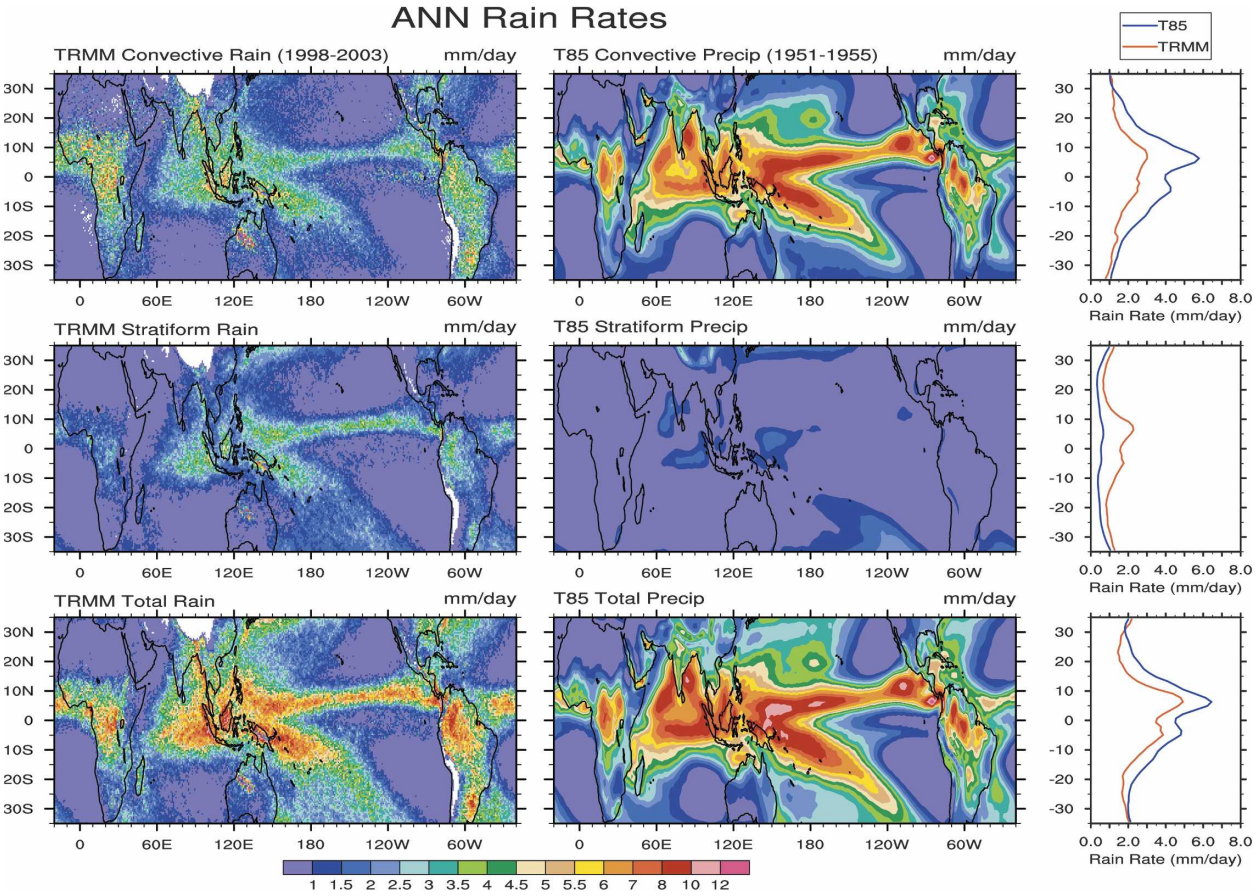

FIG. 1. Annual average of convective and stratiform precipitation estimates from TRMM at T85 resolution and CAM3 at T85 resolution.

model is sensitive to resolution. The T31 and T42 simulations show much less stratiform rain in the Tropics (not shown). Dai and Trenberth (2004) suggested that the underestimate of stratiform precipitation in CCSM2 was related to deficiencies in the moist convection scheme. They hypothesized that moist convection occurred too frequently and lasted too long, removing water vapor prematurely and too efficiently. We show that this hypothesis is consistent with CAM3 behavior as well in section 6.

4. Issues of interannual variability

Any analysis of short-time-scale cloud features is complicated by issues of interannual variability. In our case, the differences in variability associated with regime change and the simultaneous existence of clouds with differing characteristics are the issue. As an example, Fig. 2 shows the behavior of a number of fields at a single grid point in space for two consecutive seasons of the months of December, January, and February (DJF) in a T42 configuration of the model. This model uses SSTs from a climatology constructed by taking the ensemble average of approximately 20 yr worth of monthly mean observed SST data. Therefore, the SSTs repeat annually and interannual variability from external forcing (e.g., ENSO) cannot explain the variation in the simulation.

The point of focus is located near 1°S, 45°E, in the south Indian Ocean, just off the African coast. The Indian Ocean is a region of high interannual variability in circulation and cloud properties in the real world (see, e.g., Loschnigg and Webster 2000 or Bajuk and Leovy 1998) and in our model. The upper panels of the figure show time series (at 3-h intervals) of the vertical integral of the cloud condensate mass in the column (liquid water path), low cloud fraction, convective precipitation, and stratiform precipitation for that model grid point. The liquid water path represents the average value within the column including cloudy and cloud-free areas. The lower panels show diurnal cycle composites derived by determining the local hour of the day

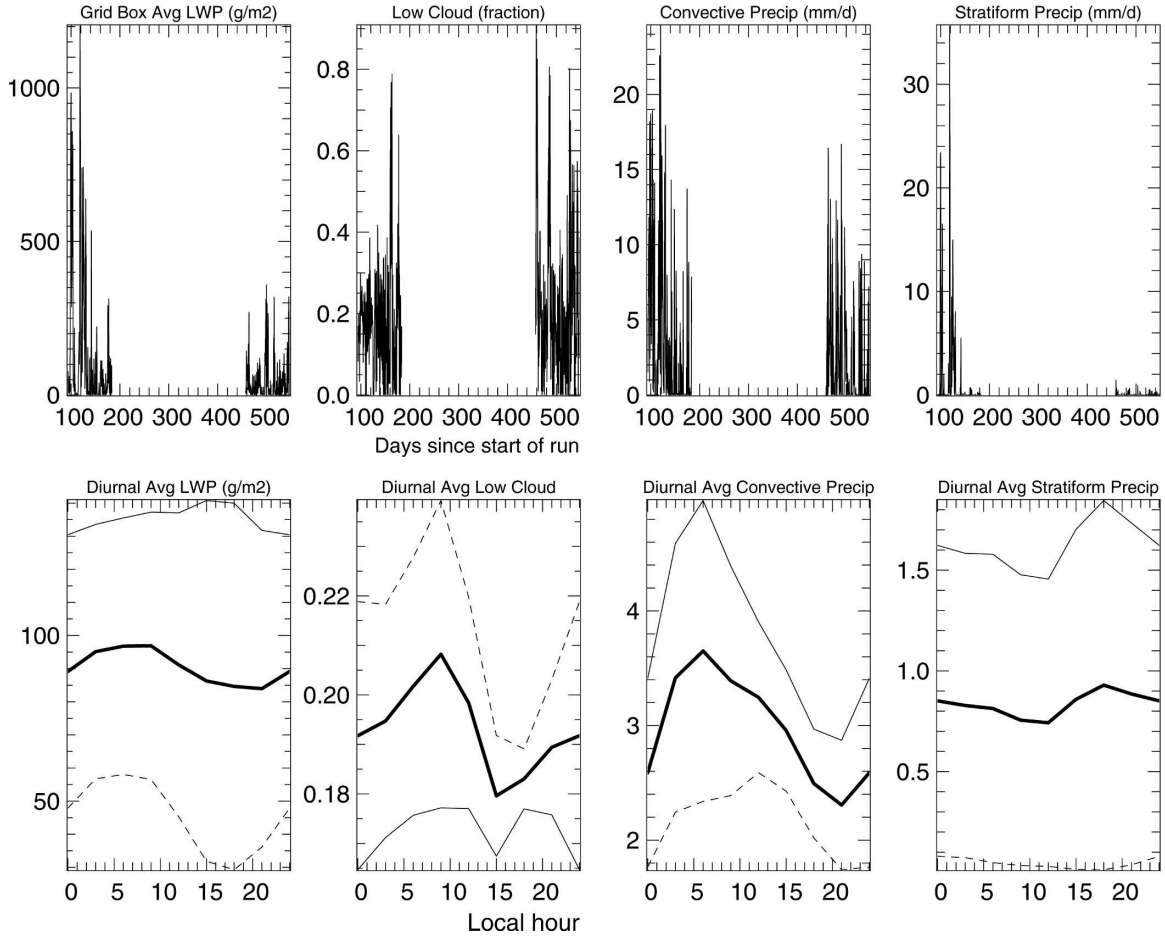

FIG. 2. (top) The time series of various fields for two adjacent DJF seasons at one model grid point. The time is in days with origin at the beginning of the model run. (bottom) The composite diurnal average for each of the seasons. The thin solid line is the average for the first season. The dashed line is the second season. The thick solid line represents the average of the two seasons.

for each time sample, and averaging all time samples with that particular local hour value. In the lower panels, we have partitioned the diurnal cycle composites three ways: an average diurnal cycle for DJF (year 1, thin, solid line); an average value for DJF (year 2, dashed line); and the average value for years 1 and 2 combined (thick, solid line). A number of interesting features are evident in the figure.

- The behavior of DJF (year 1) is different from that of DJF (year 2). Ratios of the mean value during DJF (year 1) and the mean value during DJF (year 2) vary substantially for each field, DJF (year 1) being characteristically 2–4 times higher than DJF (year 2), and the phase of the diurnal variation is also quite different.
- Stratiform rain in CAM3 is not always small in the Tropics, as can be seen in Fig. 2 (top). The maximum in instantaneous stratiform rain is actually higher than the convective rain at some times during DJF (year 1, about day 120).
- The diurnal cycle inferred separately from the two years differ from each other. Year 1 is characterized by high LWP and stratiform drizzle in the afternoon, at about 15–17 Local Solar Time (LST); high convective precipitation and cloud cover occur in the early morning. Year 2 shows maximum LWP, cloud cover, and stratiform precipitation in the early morning hours (4–6 LST), and highest convective precipitation in the early afternoon.
- The composite of the two seasons combined is a confusing meld of the two individual years. The diurnal cycle of the LWP and stratiform and convective precipitation reflect the character of year 1, while the cloud cover variations reflect the character of year 2.
- While we have not performed a formal error characterization in this figure, one could utilize the "year 1" and "year 2" estimates to be a crude estimate of the

error in the mean of the two years, in which case the error bars would span the range defined by the year-1 and year-2 estimates.

The distinctly different diurnal behavior between year 1 and year 2 suggests shifts in climatological features at that location. During year 1 the model's behavior is reminiscent of an area of strong convective activity with precipitation peaking in early morning hours and cloud optical depth/thickness peaking in early afternoon. During year 2, the model grid point looks more like a stratocumulus region, with lower precipitation rates, and a peak in cloud optical thickness in the early morning hours. The existence of more than one type of cloud behavior has previously been recognized as important in the characterization of tropical oceanic convection (Meisner and Arkin 1987; Janowiak et al. 1994; Yang and Slingo 2001).

This suggests that a desirable strategy in characterizing atmospheric transients is to stratify the data in some manner prior to the data reduction, analysis, or compositing, to isolate particular phenomena of interest. Hendon and Woodberry (1993) utilized a Deep Convective Activity (DCA) index defined as to be nonzero only where cold, optically thick clouds were present in a scene in order to identify times and locations of vigorous convection. Ricciardulli and Sardeshmukh (2002) used only months in which DCA was nonzero at least 5% of the time in their analysis of convection using the Global Cloud Imagery (GCI) dataset described below in order to focus their attention only on rain events rather than seasonal variation of the spatial patterns of rain. We have explored a variety of mechanisms in our attempts to stratify the data. When these strategies result in a clarification of the interpretation we discuss them. Otherwise, we show analyses based on 5-yr averages/composites of the data in the rest of this paper.

5. Brightness temperature analysis

There are obvious difficulties in global characterizations of the higher-frequency components of clouds, precipitation, and convection, using rain gauges, instruments with a narrow field of view on a precessing orbit, or sun-synchronous satellites. One of the most frequently used and most useful quantities for characterization of clouds is the 11-μm brightness temperature (hereafter T_{11}^B). The brightness temperature in the infrared window region (10.2–12.2 μm) provides a well-understood measure of the temperature at the top of optically thick clouds. The brightness temperature has been used as a way to characterize diurnal variability of clouds (Salby et al. 1991; Bergman and Salby 1996; Yang and Slingo 2001), deep convective activity (Hendon and Woodberry 1993; Bergman and Salby 1994), precipitation (Richards and Arkin 1981; Adler and Negri 1988; Arkin and Meisner 1987; Huffman et al. 1997), and many other cloud aspects.

Here, we use the GCI observational estimates of T_{11}^B from Salby et al. (1991). The version of the dataset we used is discussed in Ricciardulli and Garcia (2000) and Ricciardulli and Sardeshmukh (2002). This dataset includes intercalibrated measurements from four geostationary and two polar-orbiting satellites. The dataset contains synoptic estimates of global cloud fields at 3-h intervals between 1983 and 1992 at about a half-degree resolution. There are occasional missing data periods in this dataset. When there are occasional missing single time samples, these are replaced with the interpolated values from the time sample on either side of the missing sample. To avoid problems with interpretations of this field at the substantially different resolutions of the model and the GCI dataset, we produce an area-weighted mean T_{11}^B at two model resolutions, T85 (approximately 1.4° in latitude and longitude), and T42 (approximately 2.8° in latitude and longitude). Like Yang and Slingo (2001), we focus on both precipitation and T_{11}^B as useful quantities in interpreting transients features of the tropical atmosphere.

Minnis et al. (1991) showed that extremely high correlations exist between narrowband and broadband total longwave fluxes and showed that a quadratic relationship could be used to estimate the value of one from the other to an accuracy of a few percent in derived flux. We use this relationship to produce an estimate of the narrowband flux from the model top-of-atmosphere net longwave flux. The conversion from broadband to narrowband radiances is done using the relationships given in Minnis et al. (1991), which correlated infrared window (10.2–12.2 μm) data from the Geostationary Operational Environmental Satellite (GOES) with longwave (5.0–50.0 μm) data from the Earth Radiation Budget Experiment (ERBE). The best global fit for data over ocean was given by $M_b = 90.54 + 3.568M_n$ and over land by $M_b = 77.64 + 4.397M_n - 0.0111M_n^2$, where M_b and M_n are respectively broadband and narrowband estimates in W m^{-2}. First the broadband flux as predicted by the model is converted to a narrowband radiance in the 10.2–12.2-μm window used by satellites. Then the narrowband radiance is converted to an equivalent blackbody temperature. A procedure that is similar in spirit was used in Yang and Slingo (2001) following Ohring et al. (1984).

Because there are occasionally missing months in the dataset and we are restricting our analysis to shorter

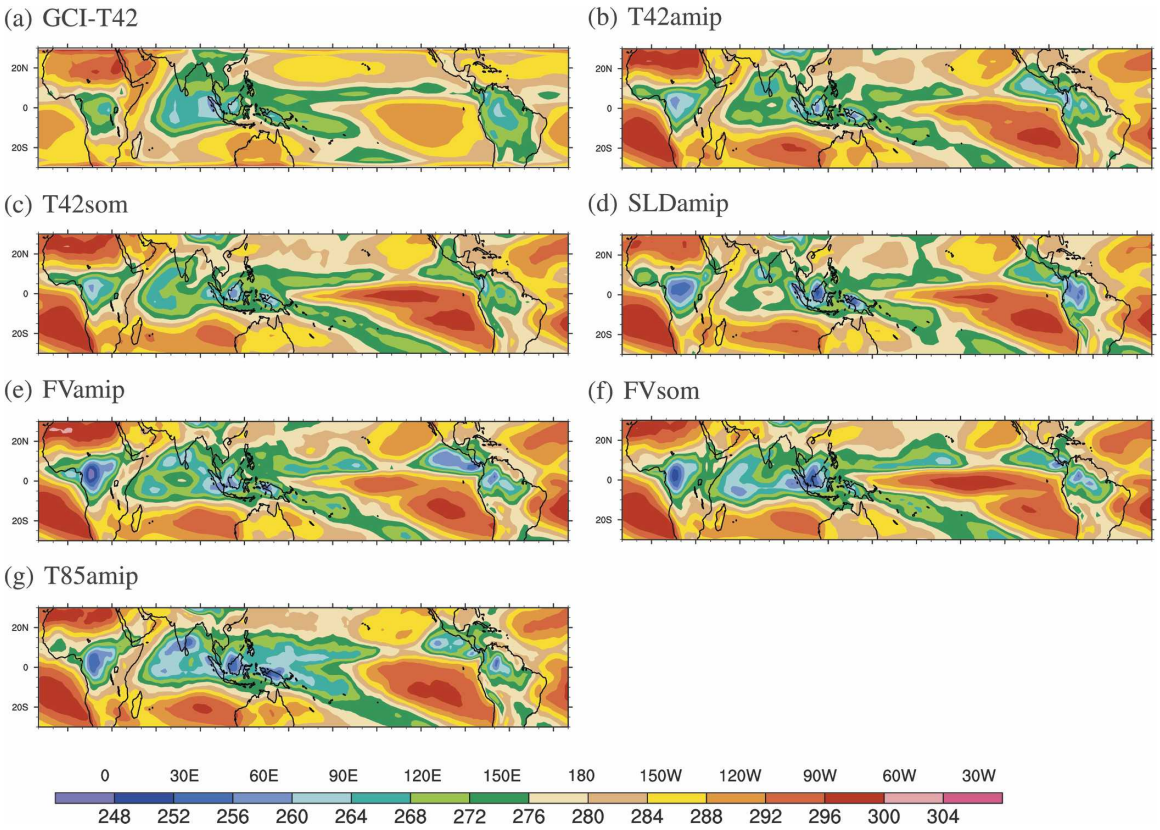

FIG. 3. Annual average T_{11}^{B} from the GCI dataset of Salby et al. (1991) and CAM3 simulations.

time scales, it is convenient to analyze each month individually, thus producing information on time scales from 6 h to ~30 days. Within each monthly dataset we calculate the time mean, the variance over all resolved frequencies, the partitioned variance (into three bins: <2 day periods, 2–10-day periods, and 10–30-day periods) and the time of maximum T_{11}^{B}. We estimate the local time of the maxima in brightness temperature by the compositing technique described in section 4, then fit a sinusoid to the first diurnal harmonic of the composite for phase and amplitude.

Given a characterization of the mean, variance, and hour of brightness temperature maximum, we then composite all realizations of a particular month (e.g., all Januarys) to form a "climatological" January. (The hour of local maximum is calculated by converting the phase shift back to coefficients of the sinusoids, averaging ensemble members, and then converting back to the phase shift.) This provides 12 monthly samples that we can use to produce annual and seasonal averages characterizing these fields by using similar averaging procedures.

A comparison of T_{BR} is shown in Fig. 3. As expected, all the models' configurations agree reasonably well with the basic features of the observations, because the field is explicitly a function of the outgoing longwave radiation (OLR), and a reasonable reproduction of the time mean OLR is one of the features the model is required to reproduce. The features are consistent with longwave cloud forcing and OLR biases described in other papers in this issue. The role of clouds in the subtropical subsidence regions is underestimated, with too little shortwave cloud forcing and too much OLR, resulting in T_{11}^{B} that is higher than observed in these regions. The role of clouds in the ITCZ regions is overestimated with too high cloud forcing and too low OLR, with too low T_{11}^{B} there.

The annually averaged estimate of total variance (the variance about the 30-day mean, based on the 3-h time samples) of T_{11}^{B} is shown in Fig. 4. The model variance increases monotonically as the resolution increases across the spectrum of model configurations. This is true regardless of whether one examines the same dynamical core (Figs. 4b,g) or between dynamical cores (Figs. 4b,d,e). Note that the semi-Lagrangian dynamics (SLD) resolve slightly smaller spatial scales than the spectral T42 models on the equivalent grid because there is no "spectral truncation" of most of the state

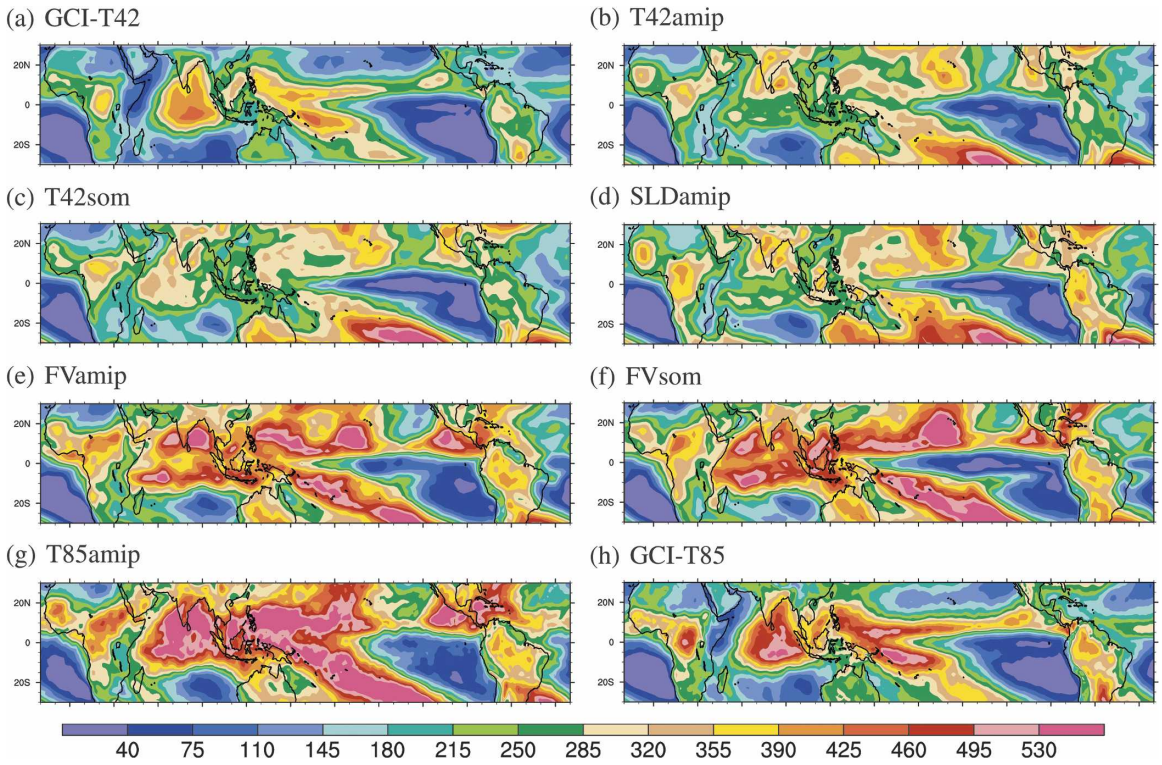

FIG. 4. Annual average of the variance of T_{11}^{B} from the GCI dataset of Salby et al. (1991) and the CAM3 simulations. Calculated from data at 3-h intervals. Units: K^2. Note that the first and last panels both show GCI data (at different spatial resolutions).

variables. The finite volume configuration has a higher resolution than either the T42 or SLD model configurations. Figures 4a,h show the observed brightness temperatures estimates calculated at the lowest model resolution (T42; top) and at the highest model resolution (T85; bottom). It is clear that the variance calculation is sensitive to resolution, as it should be, because more features are resolved as the resolution increases, but it is also apparent that the models tend to overpredict the variance compared to the GCI data at the same resolution.

The figure indicates that substantial differences between model configurations exist despite efforts to produce model configurations tuned carefully to provide a close agreement with observations in terms of seasonal and annual averages. The lower-resolution model tends to miss much of the variance seen in the areas of deepest, coldest convection [the warm pool, equatorial Indian Ocean, and South Pacific convergence zone (SPCZ)]. This is not the case for the higher-resolution configurations where the models do capture these features and indeed overestimate the variance. Near the equator, maxima in variance tend to track the minimum in time mean variance following the ITCZ. Models show areas of excessive variance in the mid-Pacific at 30°N and 30°S not seen in observational estimates.

One can avoid a focus on the biases associated with spatial patterns of the variance by examining the joint distribution functions of the mean value and variance of T_{11}^{B}. These distributions for model and GCI retrievals are shown in Fig. 5, which suggests that both observations and models have a bimodal distribution, with a very strong peak at warm brightness temperatures corresponding to a T_{11}^{B} variation near the surface, and a weaker secondary peak corresponding to clouds with a top at much higher altitudes. The higher-resolution model configurations show a nonzero variance over a broader range of temperatures than the GCI estimates. The observations have a more narrowly peaked spectrum than the model. There is no evidence for substantial difference in variance between models with interactive ocean surface temperatures (SOM) compared to fixed SSTs (see Figs. 5b,c or 5e,f for the T42 or FV model configuration, respectively).

Figures 5a,h indicate that variance is resolution dependent, since the underlying data for these figures were produced from the same high-resolution dataset, but more variance is found in the upper-left quadrant of

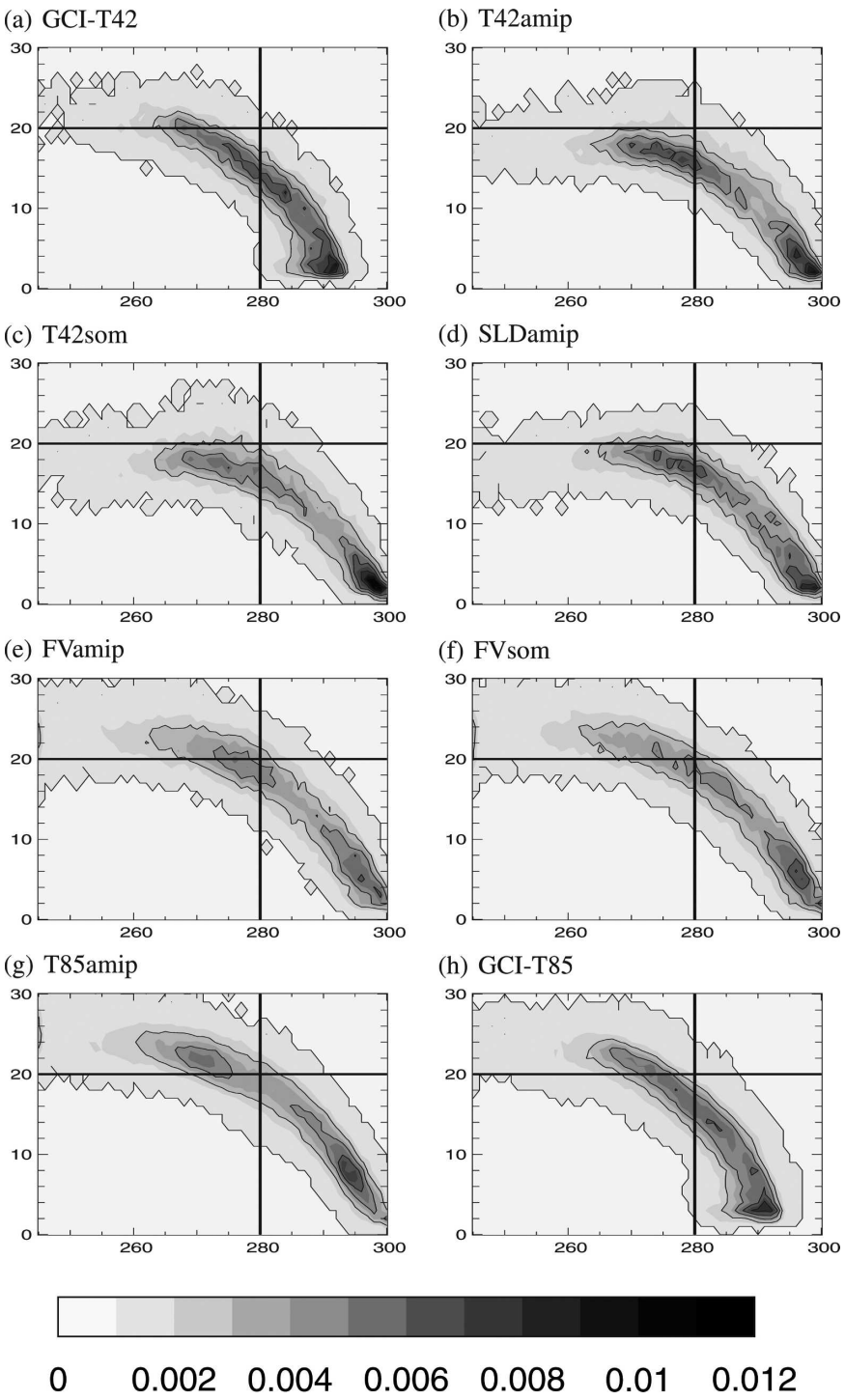

FIG. 5. Joint distribution (frequency of occurrence) plotted over oceans only between 20°N and 20°S as a function of the standard deviation of T_{11}^{B} (ordinate) and monthly mean of T_{11}^{B} (abscissa). The distribution is normalized so the integral over the area of the figure is 1. Reference axes are displayed on the figure to highlight the evolution of the local maximum associated with high cold clouds with large variance. Note that the first and last panels both show GCI data (at different spatial resolutions).

the high-resolution data (Fig. 5h) than the lower-resolution version (Fig. 5a). The same phenomenon is found in the model. The lower-resolution model (Fig. 5b) has a local maximum below the 20-K reference line while the local maximum is above that line for the equivalent high-resolution model configuration (Fig. 5g).

The total variance has been partitioned in Fig. 6 into contributions on different time scales in a manner similar to Ricciardulli and Garcia (2000). The figure indicates that the overestimate in T_{11}^{B} variance in the tropical ocean regions seen in Fig. 4 occurs primarily at time scales of 2–10 days. Variance of longer and shorter time scales over oceans is much closer to observed values. Biases in variance are largest in the warm pool region of the equatorial Pacific. Over oceans, both models and observations tend to place most of the variance at the 2–10-day time scales. There is a substantial difference between the spectral T42 and FV model configurations, while there is not much difference between simulations including and excluding the slab ocean model. This implies that our model clouds are not responding strongly to interactive surface temperature. All models tend to have too much variance at longer time scales (2–10 days), and not enough at shorter time scales (<2 days).

Over land, the simulations look much closer to the observations. The basic partitioning of variance is much closer to the observations than over oceans across all frequency intervals. The FV model configuration shows somewhat more realistic features than the spectral model simulations there.

6. Precipitation analysis

It is difficult to find reliable and robust estimates suitable for a climatological characterization of short-time-scale global precipitation events. There are vast expanses of the globe with limited availability of measurements, and the measurements in the more remote regions of the earth are frequently made as the opportunity occurs (e.g., ship track data). Dai (2001) analyzed 23 yr of 3-hourly surface weather reports to document the diurnal cycle of precipitation occurrence for various types of precipitation over the globe. Dai and Trenberth (2004) used these surface observation to evaluate the CCSM2. That dataset allowed one to categorize the frequency of occurrence of precipitation type (drizzle, showery precipitation, snow, etc.), but it did not provide a quantitative measure of the intensity of the precipitation occurring in various regions of the world by hour of day.

Although TRMM measurements provide a good measure of precipitation locally, and globally over long time scales, they are of limited utility for sampling short-time-scale phenomena. The TMI produces only about 15 samples per year of the diurnal cycle at any locale. It revisits any given area at the same time infrequently (23 days at the equator and 46 days in the extratropics). It thus provides limited information about short-time-scale variability and is able to estimate features like the diurnal cycle of precipitation only by a compositing technique produced by examining the same location of a region over a very long time (Negri et al. 2002a). A fruitful method for estimating precipitation globally has been to use TRMM to calibrate another measured quantity that can produce high-frequency retrievals of precipitation. One dataset that fits this description is the TRMM-calibrated dataset 3B42. This is a product that first uses the TMI and Visible Infrared Scanner (VIRS) infrared measurements on TRMM to calibrate the algorithm, then applies the algorithm to merged geosynchronous data to produce a global, 3-hourly dataset. The 3B42 dataset includes only the years 1998 and 1999. We have at times regridded the 3B42 dataset to various resolutions to facilitate comparisons with the model.

Figure 7 shows the precipitation variance for three model runs in a format similar to Fig. 6. Please note that the contour intervals for the model runs (Fig. 7e) were chosen to be much smaller than the color bar for the precipitation retrievals (Fig. 7f), reflecting the fact that the current model configurations substantially underestimate the variance in precipitation compared to the observational estimates. These figures may be compared to a similar set of figures in Ricciardulli and Garcia (2000, their Figs. 2 and 4), who found that CCM3 underestimated the variance in precipitation at high frequencies, and in their case, overestimated the variance in the lower frequency band. The discrepancy between observational estimates and model simulations was substantially larger in Ricciardulli and Garcia (2000), which required a change in the contour interval by a factor of 10 between model and observational estimates to produce figures showing any signal. Our analysis suggests that CAM3 and the observations differ in variance by factors of about 3 at the 2–10-day frequency interval and 4–5 in the higher frequency interval. As also seen in variance of T_{11}^{B}, discrepancies are largest over the tropical ocean. The observational estimate put most of the variance on the shortest time scales, while all model configurations reflected most of the variance in the 2–10-day time-scale interval. Figures 7b–d do show that increasing the resolution increases the model variance at the 2–10-day time scales but decreases the variance at the shorter time scales. Over land, the discrepancies are much lower; the model puts

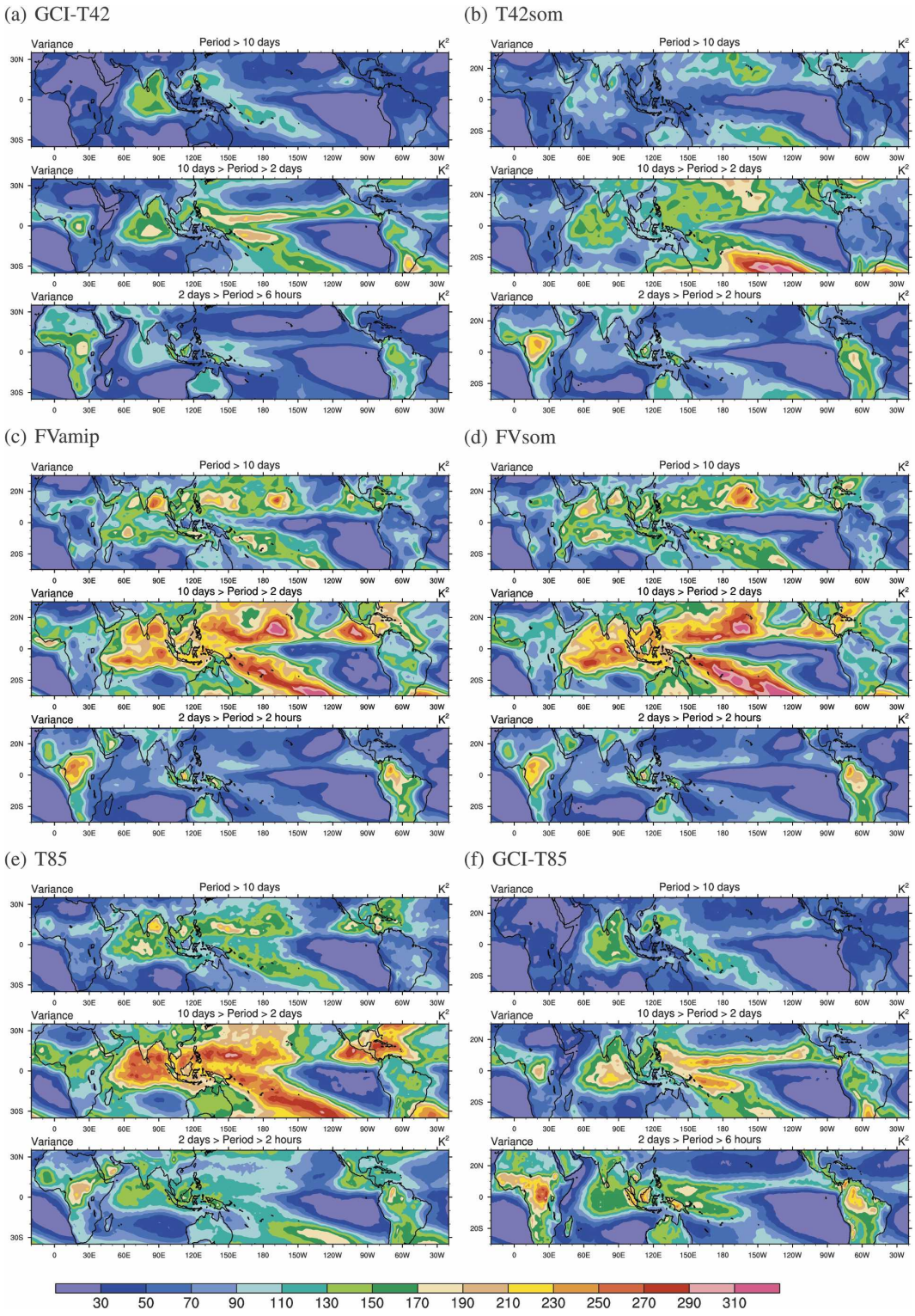

FIG. 6. Annual average of the variance of T_{11}^{B} partitioned into frequency bins from the GCI dataset of Salby et al. (1991) and the CAM3 simulations.

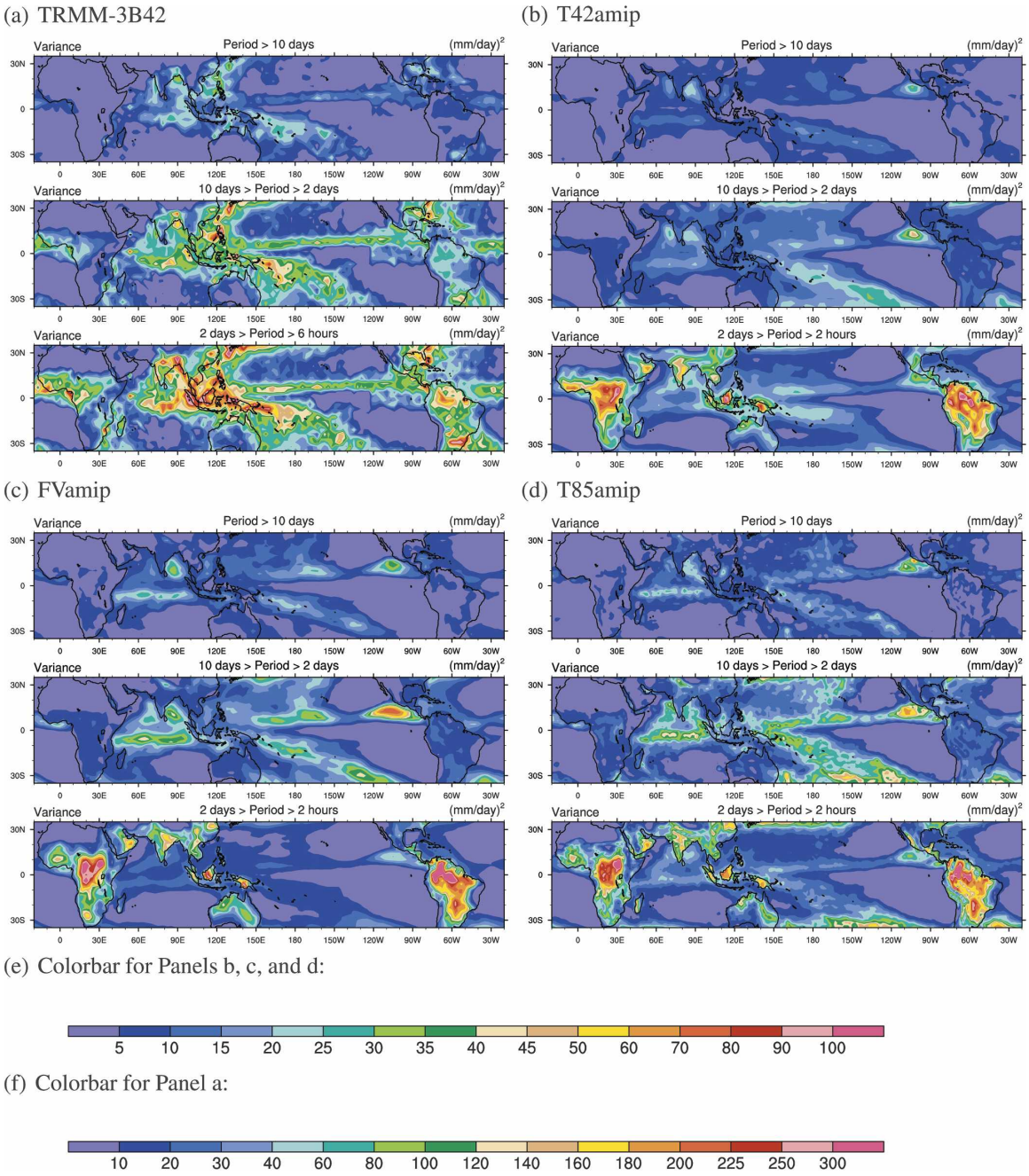

FIG. 7. Annual average of the variance precipitation partitioned into frequency bins from the (a) TRMM 3B42 dataset (at T85 resolution) and the CAM3 simulations: (b) T42amip, (c) FVamip, and (d) T85amip.

most of the variance in the shorter time-scale interval, and it is within 50% of the observational estimate.

Figure 8 shows composite diurnal cycles for six regions near the equator for June–August (JJA), at approximately the same latitude, but with quite different climatological regimes. The land regions (Africa and tropical South America) are strongly influenced by heating and cooling of the land surface. The equatorial Indian Ocean region is adjacent to and strongly influenced by the Indian monsoon. Oceanic ITCZ regions are located near the Pacific warm pool, the cold pool, and the central Atlantic Ocean, respectively. We show estimates of the diurnal cycle for the T85 model, estimates following Negri et al. (2002b) from PR and TMI, and the IR-calibrated 3B42 product. The ocean ITCZ regions all have a relatively weak diurnal variation. The

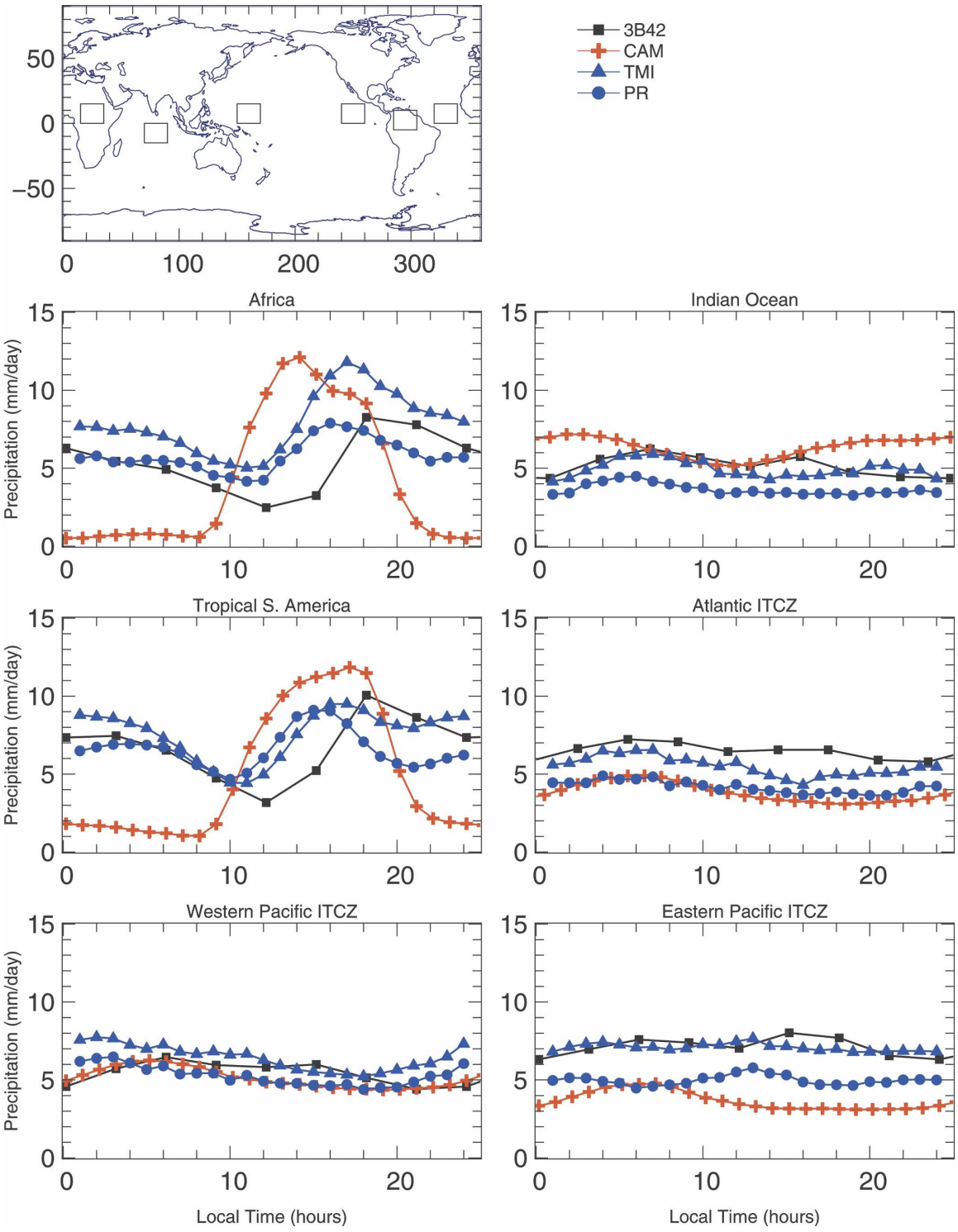

FIG. 8. Regional composites of precipitation during JJA from the T85 version of the CAM3, and three observational estimates. TMI and PR estimates utilized 6 yr of data (1998–2003). The 3B42 dataset used data for 1998–99. Five years of model simulation were used for the CAM3 estimate.

western Pacific ITCZ modeled and retrieved diurnal variation agree quite well. All show a mean value of 6–7 mm day^{-1} with an amplitude of diurnal variation of 2–3 mm day^{-1}, and the peak precipitation occurs in the early morning hours. TMI and PR show maxima between midnight and 0200 LST. The IR product and CAM3 show a maximum about 3 h later. The model and measurements agree less well over the other oceanic regions. The retrieved precipitation estimates in the eastern Pacific region tend to put the maximum value between 1000 and 1800 LST, although the signal is very weak. The amplitude and time of maximum precipitation are consistent in the Atlantic ITCZ region between model and retrieval. All the model simulations estimate the maximum to occur in the morning hours. Agreement between model and retrievals is worst for the Indian Ocean region, where the model is almost out of phase with the observations.

The continental regions show a much stronger diurnal variation. The observations show a semidiurnal variation of precipitation with an early morning peak and a late afternoon peak. The model shows only the afternoon peak, and the amplitude of the diurnal variation tends to be stronger than that seen in the retrievals. The model tends to overestimate the diurnal cycle over land. The maximum occurs too early in the day over Africa, but not over northern South America. The model tends to underestimate nighttime precipitation in these regions. The 3B42 dataset again shows a few-hour lag compared to the TMI or PR retrievals for these regions.

The spatial distribution of the amplitude and phase of the diurnal cycle of precipitation is shown in Fig. 9. To facilitate a comparison with the model, we have shifted the 3B42 estimate of time of maximum precipitation by 3 h (earlier) to compensate for the lag between IR retrieved precipitation and radar, microwave, raingauge, or other surface measurements of LST [see Janowiak et al. (1994) and discussion surrounding Fig. 8]. Figures 9c and 9d show late afternoon precipitation over large tropical landmasses, consistent in the 3B42–T85 and T85amip model runs, respectively. The model's precipitation occurs 2–4 h earlier than observations. The amplitude of the diurnal cycle of precipitation over South America is larger than observations. There is some evidence for topographic effects in the vicinity of the Andes and Ethiopia, but it is much weaker in the model than observations. The model clearly is not resolving the steep topography or the spatial scales that are known to be important in representing land/sea and mountain valley breezes. The afternoon maximum in convection is over maritime landmasses, surrounded by a morning maximum in convection off the coasts (Mapes and Houze 1993), although again, only the larger islands of the maritime subcontinent are resolved by the model, even at T85 resolutions.

Over oceans, the amplitude of the diurnal cycle is substantially underestimated, consistent with Fig. 7. The model amplitude is frequently between 0.2 and 0.3 of its mean value, while the observations suggest that it should be 0.3–0.5. The largest diurnal variation in relative terms occurs in regions where the precipitation is low, for example, stratus and stratocumulus regions. The model diurnal variation produces a smaller contribution to the total in areas of intense precipitation (ITCZ and SPCZ) and a higher contribution in subsidence regions (stratocumulus and trade cumulus regions). The same signal is seen in the 3B42 dataset (Fig. 9a), but the difference in intense rain between these regions and other areas of the globe is less pronounced than seen in the model.

Both observational estimates and the model frequently show the maximum in precipitation to occur between 2200 and 0600 LST over most of the tropical ocean. But the precipitation maximum occurs a few hours later, much more frequently in the observational estimates than in the model. Both estimates show later times for precipitation in the Bay of Bengal and near South America and the west coast of Africa (Gulf of Guinea). As seen in earlier versions of CAM3 (Dai and Trenberth 2004) the model tends to precipitate a few hours earlier over tropical landmasses than as seen in the observational estimate, with precipitation peaking between 1400 and 1600 LST in the model, and 1600 and 1800 LST in the observations.

Ricciardulli and Sardeshmukh (2002) have characterized the duration of precipitation events from observations and CCM3. We repeat one of their diagnostics using the 3B42 dataset and the T85amip, T42som, and FVsom versions of CAM3. The duration of the precipitation was calculated in the following way. An event was defined monitoring the length of time (in 3 h steps) that precipitation exceeded a threshold (1 mm/day). The average length at a grid point was then defined to be the average of the event lengths at that point.

Figure 10 (top) shows the duration of precipitation events as gauged from the 3B42 dataset. Data with drizzle (rain < 1 mm day^{-1}) have been filtered prior to the analysis to produce a clearer picture of the duration of substantial precipitation. The longest time-scale events (8–10 h) are seen in the ITCZ region of the Atlantic and Pacific Oceans. Over other parts of the tropical oceans the precipitation duration is 4–8 h. The duration of events over tropical landmasses is also 4–8 h or shorter.

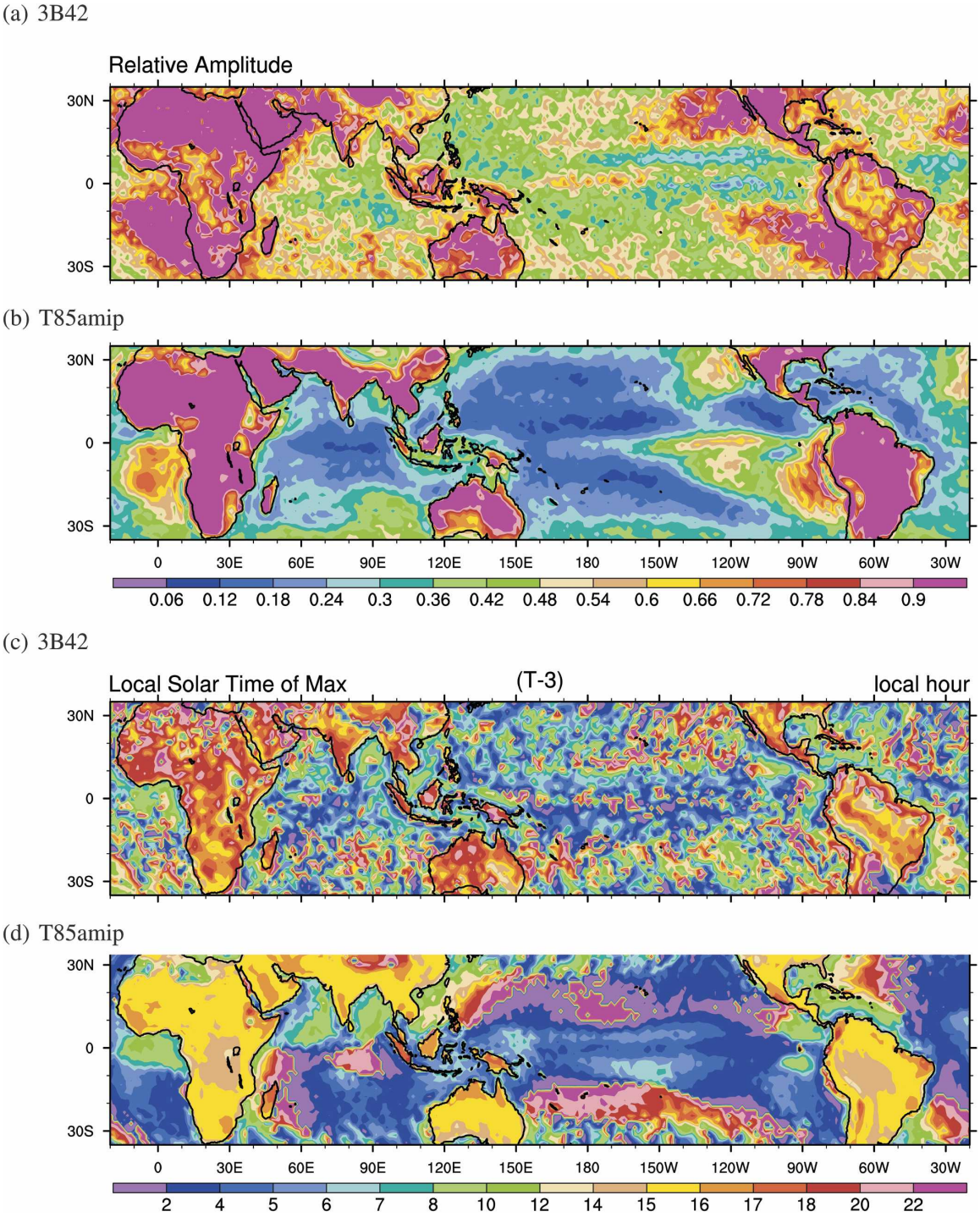

FIG. 9. Comparison of diurnal cycle of the 3B42 precipitation product and T85amip. (a), (b) The relative amplitudes of the diurnal cycle. (c), (d) LST of maximum precipitation. The LST of (c) has been shifted by 3 h to account for the known lag of IR precipitation retrievals in estimating time of maximum precipitation.

The duration of precipitation for events for all model configurations (Figs. 10b,c,d) is much longer. We have increased the color bar scale by a factor of 4 to provide information about the range of events seen in the model. Most oceanic precipitation events last as long as 36 h, with the longest events persisting for up to 72 h. Over landmasses the precipitation events are as long as 12 h.

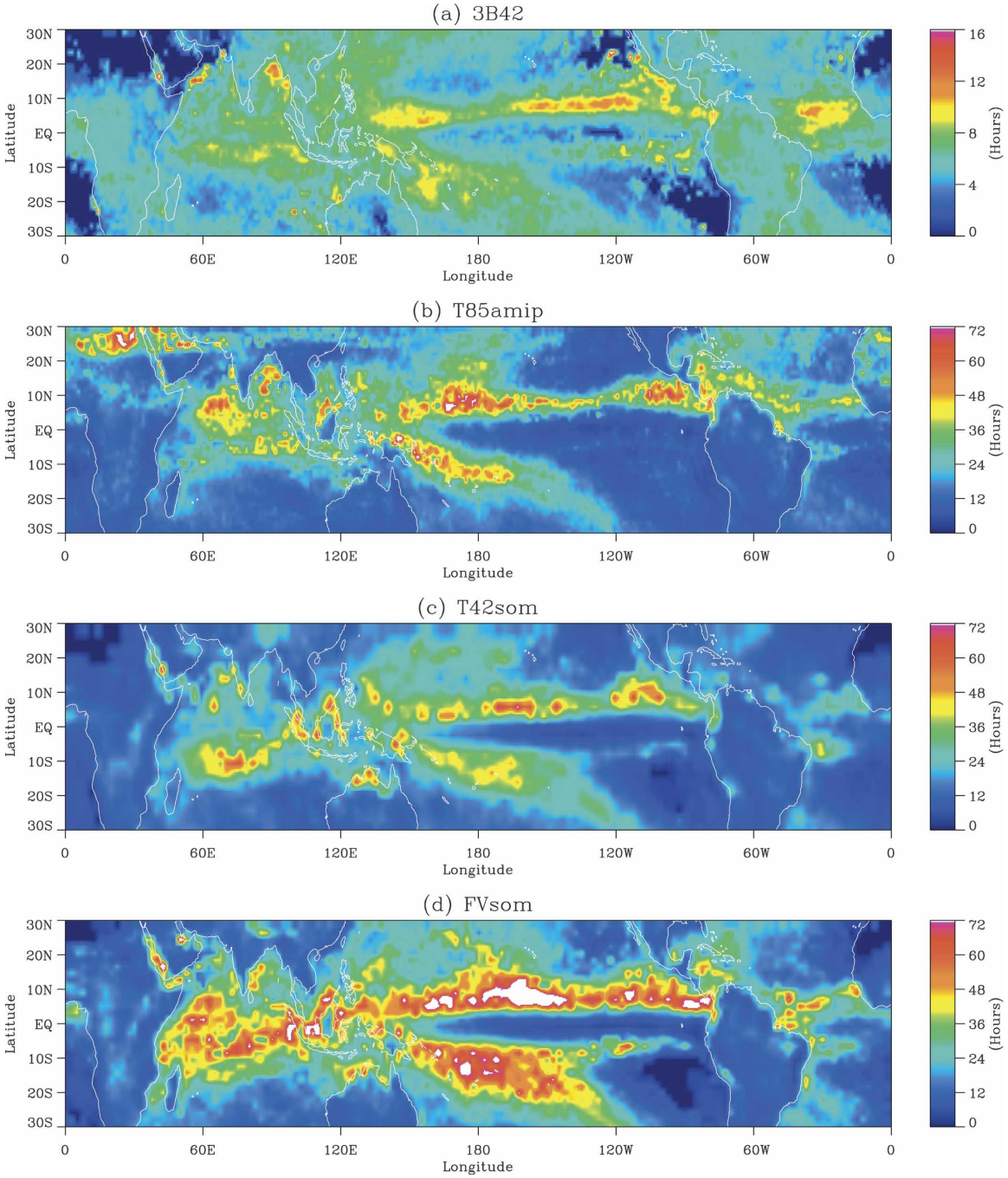

FIG. 10. Duration of precipitation events derived from 3B42 and various model configurations. Note the change in scale for the observed and modeled precipitation duration.

This figure does not address whether the transient features are propagating or the spatial coherence of the field (the analysis is done independently for each grid point). However, analysis of the fields suggest that organized structures with spatial scales consistent with observations do exist in CAM3 (not shown). The results are similar to the study of Ricciardulli and Sardeshmukh (2002). The features could be associated with dynamical features like the MJO, although this is far too weak in CAM3 (not shown).

7. Liquid water path

Wood et al. (2002) have analyzed some aspects of the diurnal cycle of the liquid water path in the Tropics and

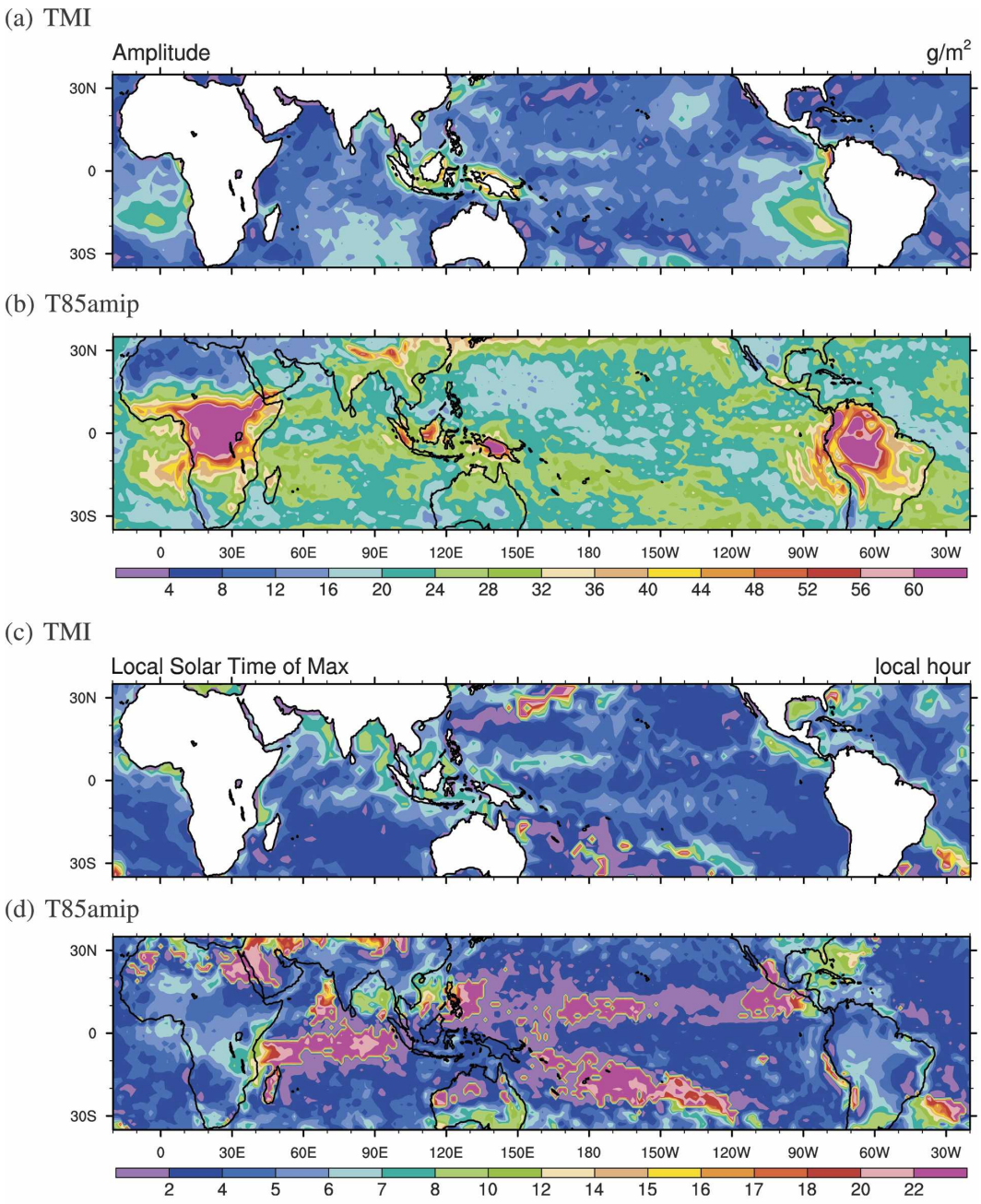

FIG. 11. (a), (b) Amplitude of LWP diurnal cycle; (c), (d) LST of maximum LWP as estimated from the TRMM TMI and the T85amip model configuration.

subtropics using TRMM TMI data with a focus on nonprecipitating boundary layer clouds. The LWP retrieval for this dataset uses the algorithm from Wentz (1997). The retrieval is performed only over ocean surfaces for nonprecipitating clouds. Figure 11 shows the amplitude of the diurnal cycle, and estimated hour of maximum LWP from this analysis, compared to the T85amip version of CAM3 (where the hour is calculated for both precipitating and nonprecipitating clouds). Both model and observations put the largest amplitude diurnal cycle in the Southern Hemisphere (off the west coast of South America and South Africa), in regions with large amounts of stratocumulus clouds. As noted by Wood et al. (2002), there is a strong asymmetry between north-

ern and southern stratocumulus regions. The amplitude of the diurnal cycle is as much as a factor of 2 higher over much of the ocean region in the model compared to the TRMM-retrieved value. It is not clear whether the exclusion of precipitating clouds in the TRMM retrieval can explain this difference. We have explored the consequences of excluding model cells in which there is no precipitation, but this dramatically reduces the liquid water path. Because the exclusion of precipitating clouds during the precipitation retrieval is done at a much finer spatial resolution, the impact may be much different than a procedure excluding the model columns at the lower resolution. Both model and observation indicate that the LST for maximum LWP occurs in the early morning (0–4) hours over most of the oceanic regions, although the model LWP maximum tends to occur an hour or two earlier than the observations. Both also show a maximum near local noon in the Caribbean and the Bay of Bengal.

8. Summary and conclusions

There are still many uncertainties in quantifying aspects of atmospheric transients associated with the hydrologic cycle. Space-based retrievals are probably accurate only to 30% or so, and many of the best of those measurements are available for only a few years, which complicates the interpretation because of strong interannual variability. In spite of these uncertainties we believe that CAM still has a long way to go for a reasonable representation of tropical transient activity on less than 30-day time scales. Our results show that the transient aspects of convection are too weak.

The variance of brightness temperature on less than 30-day time scales has a strong sensitivity to resolution in CAM3. Lower-resolution model runs underestimate the observed variability. Higher-resolution runs probably overestimate that variability and the spatial extent of that variability, which tends to be very strongly correlated with regions of strong convection over land and oceans. The transient variability is more sensitive to resolution than to the numerical method used to solve for the atmospheric dynamics and transport of water substances. The overestimate of variability in the model tends to occur at 2–10-day time scales. The shorter time scales ($<$2 days) tend to underestimate variability in the model.

The very strong connection observed between brightness temperature and precipitation in the observed atmosphere (Ricciardulli and Sardeshmukh 2002; Negri et al. 2002a) is much weaker in CAM3. The differences in transient activity as seen in the precipitation statistics and those in the brightness temperatures suggest that the linkage between the convective parameterization and the radiatively active high clouds are weaker in the model than in the real world. One can construct scenarios that explain this discrepancy as a function of the balance in the opacity of the high clouds that influence the brightness temperature with the sources from convection and the sinks from sedimentation and stratiform precipitation processes. An alternate point of view is that the tropical deep convection is not evolving in stratiform clouds according to the same mechanisms seen in the observations. These are of course just hypotheses but are avenues worthy of future investigation.

Stratiform rain in the model is shown to be about 10% of total rainfall in the Tropics, rather than the estimated 30%–60% in the real atmosphere. Dai and Trenberth (2004) suggested that the underestimate of stratiform precipitation in CCSM2 was related to deficiencies in the moist convection scheme. They hypothesized that moist convection occurred too frequently and lasted too long, removing water vapor prematurely and too efficiently. This conclusion is consistent with the study of Ricciardulli and Sardeshmukh (2002) and this study. We have shown that CAM3 precipitation events last much longer (as long as 60 h) than those inferred from the space-based retrievals at an equivalent resolution (about 12 h). These features can also be explained by positing that the precipitation is occurring as long-duration stationary events rather than organized propagating disturbances. This is also an avenue that should be looked at in future studies.

Dai and Trenberth (2004) also showed that CCSM1 had too low diurnal variations of precipitation and cloud cover over oceans and speculated that it was due in part to the use of SSTs that included no diurnal variation. We have examined model runs that include surface properties that can evolve on subdiurnal time scales, and there is little improvement in the model variability. The slab ocean model allows for a weak variation in SST, because it is intended to model the mixed layer, which is much deeper than the top few meters of the ocean that participate strongly in the diurnal variation. The result suggests that a larger variation in SST than provided by the SOM would be needed to introduce a diurnal variation in the SST, or that some other necessary condition for diurnally varying convection may also be missing. Other experiments (not shown) indicate that likely candidates are the closure and tunable parameters in the current convection scheme. Changes to the closure or replacement of the current parameterization with others result in a substantial change to the diurnal variability of the model over oceans.

Most model configurations show similar behavior in terms of the transient variability. We found a strong sensitivity of modeled T_{11}^B to resolution. The sensitivity of the modeled rainfall variability to resolution was much smaller than that of T_{11}^B. All model configurations still underestimated the precipitation variability of the atmosphere over oceans. The underestimation is most severe at time scales shorter than 2 days, but the model variability is also too low on 2–10-day time scales. We estimate that the model is a factor of 3–5 too low in terms of the amplitude of the diurnal cycle of precipitation, which shows less discrepancy with observations than earlier versions of the model but is still distressingly large. Increasing resolution does increase the variability in the precipitation fields, but it is not a viable solution to improving the lack of variance of the precipitation. Some other measure must be found. The maximum rainfall rate over oceans tends to occur in the early morning hours in both the model and the atmosphere, but (as in the studies with CAM3's predecessors) the model peak comes a few hours earlier than the estimates for the atmosphere.

The diurnal variation over tropical landmasses is represented more faithfully than over oceans in the model. The model still tends to overestimate the amplitude of the diurnal cycle, and it tends to rain too much during the day and not enough at night.

Our results suggest that the model overestimates the diurnal variation of LWP, but because the retrieval of LWP was not done when precipitation is present, the TRMM estimate may be underestimating the amplitude of the diurnal cycle by excluding clouds with the largest liquid water contents. (The TRMM TMI instrument retrieval uses information at about a 10-km footprint.) The largest diurnal variations in cloud LWP in the model and observations are seen in the Southern Hemisphere off the west coast of the continents in regions typically occupied by stratocumulus clouds. Peak LWP occurred later in the day in the Bay of Bengal and Caribbean. We did not attempt to identify the contributions to the LWP from variations of in-cloud water content versus cloud fraction.

It is clear that while there is a strong spatial correlation between T_{11}^B variance and precipitation variance in the model, there is not a very strong correlation between brightness temperature and precipitation themselves in the model. The strong correlation between these fields in nature is the reason that IR retrieval techniques are so successful in producing accurate estimates of precipitation. This inconsistency in model behavior may serve as an indicator of "missing links" and what processes could be improved in the model.

In previous generations of the CAM most of our attention has been focused on developing a model that provides reasonable fidelity to the atmosphere on seasonal, annual, and interannual time scales. These features remain important, but it is clear that there are other meteorological features occurring at shorter time scales that we know to be important that are still poorly handled in the model. Our intention is to begin examining these features routinely in the ongoing effort to develop the next generation of CAM.

Acknowledgments. We thank Danielle Coleman and Jim McCaa for assistance in model runs and data analysis, and Christina Book for editorial assistance. We benefited greatly from conversations with George Huffman and Tom Bell regarding TRMM data, PDFs, and general caveats about interpretation of satellite data. We thank Murray Salby for providing the GCI dataset, and George Kiladis and an anonymous reviewer for their constructive comments.

REFERENCES

Adler, R. F., and A. J. Negri, 1988: A satellite infrared technique to estimate tropical convective and stratiform rainfall. *J. Appl. Meteor.,* **27,** 30–51.

Arkin, P. A., and B. N. Meisner, 1987: The relationship between large-scale convective rainfall and clod cloud over the Western Hemisphere during 1982–84. *Mon. Wea. Rev.,* **115,** 51–74.

Bajuk, L. J., and C. B. Leovy, 1998: Seasonal and interannual variations in stratiform and convective clouds over the tropical Pacific and Indian Oceans from ship observations. *J. Climate,* **11,** 2922–2941.

Bergman, J. W., and M. L. Salby, 1994: Equatorial wave activity derived from fluctuations in observed convection. *J. Atmos. Sci.,* **51,** 3791–3806.

——, and ——, 1996: Diurnal variations of cloud cover and their relationship to climatological conditions. *J. Climate,* **9,** 2802–2819.

Boville, B. A., P. J. Rasch, J. J. Hack, and J. R. McCaa, 2006: The representation of clouds and precipitation processes in the Community Atmosphere Model version 3 (CAM3). *J. Climate,* **19,** 2184–2198.

Bowman, K. P., A. B. Phillips, and G. R. North, 2003: Comparison of TRMM rainfall retrievals with rain gauge data from the TAO/TRITON buoy array. *Geophys. Res. Lett.,* **30,** 1757, doi:10.1029/2003GL017552.

Collier, J. C., and K. P. Bowman, 2004: Diurnal cycle of tropical precipitation in a general circulation model. *J. Geophys. Res.,* **109,** D17105, doi:10.1029/2004JD004818.

Collins, W. D., and Coauthors, 2004: Description of the NCAR Community Atmosphere Model: CAM3.0. Tech. Rep. NCAR/TN-464+STR, National Center for Atmospheric Research, Boulder, CO, 226 pp. [Available online at http://www.ccsm.ucar.edu/models/atm-cam.]

——, and Coauthors, 2006: The formulation and atmospheric simulation of the Community Atmosphere Model version 3 (CAM3). *J. Climate,* **19,** 2144–2161.

Dai, A., 2001: Global precipitation and thunderstorm frequencies. Part II: Diurnal variations. *J. Climate,* **14,** 1112–1128.

——, and K. E. Trenberth, 2004: The diurnal cycle and its depiction in the Community Climate System Model. *J. Climate,* **17,** 930–951.

Denning, A., D. Randall, G. Collatz, and P. Sellers, 1996: Simulations of terrestrial carbon metabolism and atmospheric CO_2 in a general circulation model. Part 2: Spatial and temporal variations of atmospheric CO_2. *Tellus,* **48B,** 543–567.

Hack, J. J., J. M. Caron, G. Danabasoglu, K. W. Oleson, C. Bitz, and J. E. Truesdale, 2006a: CCSM–CAM3 climate simulation sensitivity to changes in horizontal resolution. *J. Climate,* **19,** 2267–2289.

——, ——, S. G. Yeager, K. W. Oleson, M. M. Holland, J. E. Truesdale, and P. J. Rasch, 2006b: Simulation of the global hydrological cycle in the CCSM Community Atmosphere Model version 3 (CAM3): Mean features. *J. Climate,* **19,** 2199–2221.

Hartmann, D. L., H. H. Hendon, and R. A. Houze Jr., 1984: Some implications of the mesoscale circulations in tropical cloud clusters for large-scale dynamics and climate. *J. Atmos. Sci.,* **41,** 113–121.

Hendon, H. H., and K. Woodberry, 1993: The diurnal cycle of tropical convection. *J. Geophys. Res.,* **98,** 16 623–16 637.

Houze, R. A., 1997: Stratiform precipitation in regions of convection: A meteorological paradox? *Bull. Amer. Meteor. Soc.,* **78,** 2179–2196.

——, C. C. Heng, C. A. Leary, and J. F. Gamache, 1980: Diagnosis of cloud mass and heat fluxes from radar and synoptic data. *J. Atmos. Sci.,* **37,** 754–773.

Huffman, G. J., R. F. Adler, A. Chang, R. Ferraro, A. Gruber, A. McNab, B. Rudolf, and U. Schneider, 1997: The Global Precipitation Climatology Project (GPCP) combined precipitation dataset. *Bull. Amer. Meteor. Soc.,* **78,** 5–20.

Janowiak, J., P. A. Arkin, and M. Morrissey, 1994: An examination of the diurnal cycle in oceanic tropical rainfall using satellite and in situ data. *Mon. Wea. Rev.,* **122,** 2296–2311.

Jorgensen, D. P., and M. A. LeMone, 1989: Vertical velocity characteristic of oceanic convection. *J. Atmos. Sci.,* **46,** 621–640.

Kiehl, J. T., C. Shields, J. J. Hack, and W. D. Collins, 2006: The climate sensitivity of the Community Climate System Model version 3 (CCSM3). *J. Climate,* **19,** 2584–2596.

Kummerow, C., and Coauthors, 2000: The status of the Tropical Rainfall Measuring Mission (TRMM) after two years in orbit. *J. Appl. Meteor.,* **39,** 1965–1982.

LeMone, M. A., and E. J. Zipser, 1980: Cumulonimbus vertical velocity events in GATE. Part I: Diameter, intensity and mass flux. *J. Atmos. Sci.,* **37,** 2444–2457.

Loschnigg, J., and P. J. Webster, 2000: A coupled ocean–atmosphere model of SST modulation for the Indian Ocean. *J. Climate,* **13,** 3342–3352.

Mapes, B. E., and R. A. Houze Jr., 1993: Cloud clusters and superclusters over the oceanic warm pool. *Mon. Wea. Rev.,* **121,** 1398–1415.

Masunaga, H., T. Iguchi, R. Oki, and M. Kachi, 2002: Comparison of rainfall products derived from TRMM Microwave Imager and precipitation radar. *J. Appl. Meteor.,* **41,** 849–862.

Meisner, B. N., and P. A. Arkin, 1987: Spatial and annual variations in the diurnal cycle of large-scale tropical convective cloudiness and precipitation. *Mon. Wea. Rev.,* **115,** 2009–2031.

Minnis, P., D. F. Young, and E. F. Harrison, 1991: Examination of the relationship between outgoing infrared window and total longwave fluxes using satellite data. *J. Climate,* **4,** 1114–1133.

Negri, A. J., R. F. Adler, and L. Xu, 2002a: A TRMM-calibrated infrared rainfall algorithm applied over Brazil. *J. Geophys. Res.,* **107,** 8048, doi:10.1029/2000JD000265.

——, T. Bell, and L. Xu, 2002b: Sampling of the diurnal cycle of precipitation using TRMM. *J. Atmos. Oceanic Technol.,* **19,** 1333–1344.

Ohring, G., A. Gruber, and R. Ellingson, 1984: Satellite determinations of the relationship between total longwave radiation flux and infrared window radiance. *J. Climate Appl. Meteor.,* **23,** 416–425.

Rasch, P. J., D. B. Coleman, N. Mahowald, D. L. Williamson, S.-J. Lin, B. A. Boville, and P. Hess, 2006: Characteristics of atmospheric transport using three formulations for atmospheric dynamics in a single GCM framework. *J. Climate,* **19,** 2243–2266.

Rayner, N. A., D. E. Parker, E. B. Horton, C. K. Folland, L. V. Alexander, and D. P. Powell, 2003: Global analyses of sea surface temperature, sea ice, and night marine air temperature since the late nineteenth century. *J. Geophys. Res.,* **108,** 4407, doi:10.1029/2002JD002670.

Reynolds, R., N. Rayner, T. Smith, D. Stokes, and W. Wang, 2002: An improved in situ and satellite SST analysis for climate. *J. Climate,* **15,** 1609–1625.

Ricciardulli, L., and R. Garcia, 2000: The excitation of equatorial waves by deep convection in the NCAR Community Climate Model. *J. Atmos. Sci.,* **57,** 3461–3487.

——, and P. D. Sardeshmukh, 2002: Local time- and space scales of organized tropical deep convection. *J. Climate,* **15,** 2775–2789.

Richards, F., and A. Arkin, 1981: On the relationship between satellite-observed cloud cover and precipitation. *Mon. Wea. Rev.,* **109,** 1081–1093.

Salby, M. L., H. H. Hendon, K. Woodberry, and K. Tanaka, 1991: Analysis of global cloud imagery from multiple satellites. *Bull. Amer. Meteor. Soc.,* **72,** 467–480.

Schumacher, C., and R. A. Houze, 2003: Stratiform rain in the Tropics as seen by the TRMM precipitation radar. *J. Climate,* **16,** 1739–1756.

Scinocca, J. F., and N. McFarlane, 2004: The variability of modeled tropical precipitation. *J. Atmos. Sci.,* **61,** 1993–2015.

Song, X., and R. Yu, 2004: Underestimated tropical stratiform precipitation in the National Center for Atmospheric Research (NCAR) Community Climate Model (CCM3). *Geophys. Res. Lett.,* **31,** L24101, doi:10.1029/2004GL021292.

Takahashi, M., 1999: Simulation of the quasi-biennial oscillation in a general circulation model. *Geophys. Res. Lett.,* **26,** 1307–1310.

Wentz, F. J., 1997: A well-calibrated ocean algorithm for special sensor microwave/imager. *J. Geophys. Res.,* **102,** 8703–8718.

Wood, R., C. S. Bretherton, and D. L. Hartmann, 2002: Diurnal cycle of liquid water path over the subtropical and tropical ocean. *Geophys. Res. Lett.,* **29,** 2092, doi:10.1029/2002GL015371.

Yang, G.-Y., and J. Slingo, 2001: The diurnal cycle in the Tropics. *Mon. Wea. Rev.,* **129,** 784–801.